Stress generated modifications of epitaxial ferroelectric $SrTiO_3$ films on sapphire

E. Hollmann, J. Schubert, R. Kutzner, and R. Wördenweber

Citation: Journal of Applied Physics **105**, 114104 (2009);
View online: https://doi.org/10.1063/1.3139292
View Table of Contents: http://aip.scitation.org/toc/jap/105/11
Published by the American Institute of Physics

Stress generated modifications of epitaxial ferroelectric $SrTiO_3$ films on sapphire

E. Hollmann, J. Schubert, R. Kutzner, and R. Wördenweber[a)]
Institute of Bio- and Nanosystems (IBN) and JARA-Fundamentals of Future Information Technology, Forschungszentrum Jülich GmbH, D-52425 Jülich, Germany

(Received 2 March 2009; accepted 26 April 2009; published online 8 June 2009)

The effect of lattice-mismatch induced stress upon the crystallographic structure, strain, strain relaxation, and the generation of different types of defects in heteroepitaxially grown $SrTiO_3$ films on CeO_2 buffered sapphire is examined. Depending on the thickness of the $SrTiO_3$ layer, characteristic changes in the structural perfection of the layers, their crystallographic orientation with respect to the substrate system, and their strain is observed. For thin films misfit dislocations partially compensate the stress in the $SrTiO_3$ layer, whereas cracks develop in thicker $SrTiO_3$ films. The cracks are orientated along two predominant crystallographic orientations of the sapphire. The structural modifications and the formation of misfit defects and cracks are explained in a model based on lattice misfit induced stress, on the one hand, and energy considerations taking into account the stress release due to crack formation and the energy necessary for the formation of new surfaces at the crack, on the other hand. The impact of lattice misfit is discussed in two steps, i.e., intrinsic and thermal induced misfits during heteroepitaxial film growth at a given temperature and the subsequent cooling of the sample, respectively. The comparison of the theoretical predictions and the experimental observations demonstrate that intrinsic mismatch and thermal mismatch have to be considered in order to explain strain dependent effects in complex heteroepitaxial layer systems such as induced ferroelectricity of $SrTiO_3$ on sapphire. © *2009 American Institute of Physics*. [DOI: 10.1063/1.3139292]

I. INTRODUCTION

Pseudomorph strained-layer epitaxial growth has fast turned from a curiosity into a major technology for advanced semiconductor devices and for structures for solid state research. It has been demonstrated that mechanical strain can have dramatic effects on the electromagnetic properties of thin films. For instance strain-induced shifts in magnetic,[1] superconducting,[2] or ferroelectric,[3–9] transitions have been reported. For instance, for the incipient ferroelectric oxide $SrTiO_3$ (STO), a ferroelectric transition can be induced and an enhancement in the transition temperature T_c up to room temperature has been reported.[8,9] For epitaxially grown thin films, the strain is naturally induced by the underlying substrate (so-called clamping effect). The strain is caused by the lattice mismatch and the differences in thermal expansion coefficients between the substrate and the STO film.

In a previous paper[10] we reported on induced ferroelectricity of STO films that were epitaxially grown onto the microwave suitable substrate sapphire. For this system, ferroelectricity was observed up to $T_c \approx 200$ K (see Fig. 1). These observations could not be explained by the structural analysis obtained from room temperature x-ray diffraction (XRD) measurements that did not show any significant in-plain strain for room temperature. In this paper, we demonstrate, that strain has to be present in STO films on sapphire. Careful structural analysis of thin epitaxial STO films shows a rotation of the STO lattice with respect to the sapphire lattice that is accompanied by an in-plane distortion of the cubic STO lattice. For thicker films the tension is released via formation of cracks along distinctive crystalline directions. Both the distortion of the STO lattice and the development of cracks are clear indications for the presence of strain in STO films on sapphire and verify the explanation of the strain-induced ferroelectricity of STO on sapphire.[9]

II. EXPERIMENT AND DISCUSSION

The series of STO films is grown on CeO_2 buffered r-cut sapphire (Al_2O_3). In order to provide similar growth condi-

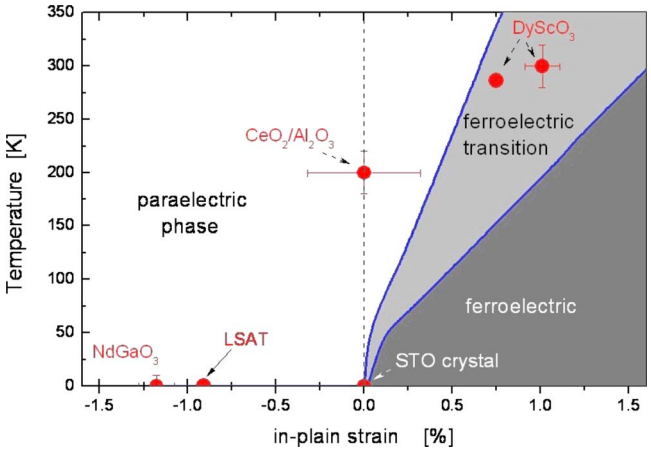

FIG. 1. (Color online) Shift in the ferroelectric transition temperature T_c of (001)-oriented STO as function of the in-plane lattice mismatch between substrate (or buffer) and STO layers. (Refs. 8 and 9) The structural mismatch was measured at room temperature, and the ferroelectricity was determined for electric field parallel to the film surface. Theoretical predictions are added. (Ref. 11)

a)Author to whom correspondence should be addressed. Electronic mail: r.woerdenweber@fz-juelich.de.

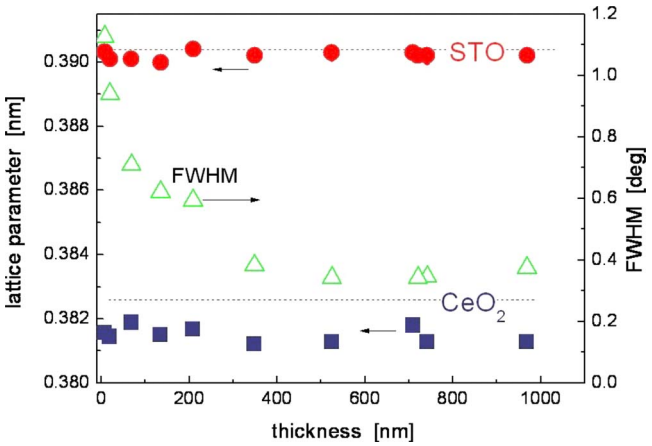

FIG. 2. (Color online) Thickness dependence of the out-of-plane lattice parameter of STO (circles) and CeO_2 (a_p, squares), and FWHM (triangles) of the (200) rocking curve of the STO layer, respectively. The dashed lines indicate the literature values of the lattice parameters for STO and CeO_2.

tions, all STO layers are deposited at identical conditions. First, a 30 nm thick [001]-oriented CeO_2 film is deposited via magnetron sputtering onto a 2 in. r-cut sapphire wafer. The wafer is cut (10×10 mm^2 pieces) and subsequently, [001]-oriented STO is deposited via pulsed laser deposition. The growth parameter (heater temperature: 850 °C, process gas: O_2 at a pressure of 1 Pa, laser power at the target: ~5 J/cm^2, and repetition rate: 10 Hz) result in a growth rate of 180 nm/min and a [001] orientation of the STO layer. STO films with thicknesses up to 1 μm are prepared

CeO_2 possesses a cubic fluoritetype structure with lattice constant $a=b=c=0.5411$ nm.[12] Epitaxial (001) STO is expected to grow with its [100] direction in [110] direction of the (001) CeO_2, i.e., the in-plane crystalline orientations of STO and CeO_2 are rotated by $\varphi=45°$ with respect to each other. As a result, STO experiences an effective cubic CeO_2 lattice with a constant $a_p\approx a/\sqrt{2}$ with $a_p\approx0.3826$ nm. The resulting nominal lattice mismatch between CeO_2 and STO films is −2.0%.

Figure 2 shows the nominal lattice mismatch (dotted lines) and the out-of-plane lattice parameters of CeO_2 and STO that are experimentally determined via XRD measurements executed at room temperature. The out-of-plane lattice parameter of the STO layers agrees nicely with the literature value of 0.3904 nm. The deviation between experimental and literature value is small (<0.05%), it could be caused by defects in the STO layer, e.g., oxygen vacancies. In contrast, all CeO_2 buffer layers show a slightly smaller lattice constant compared to the literature value. The deviation is on the order of −0.25% (which is still small). It could be a result of the lattice mismatch between CeO_2 and STO. The CeO_2 layer is very thin and exposed to the mismatch strain between sapphire and STO. A reduced out-of-plane lattice parameter is generally compensated by an enhanced in-plane lattice parameter. Thus, the reduced off-axis parameter indicates that the in-plane lattice mismatch between sapphire and STO is reduced by a small distortion of the CeO_2.

The remaining stress induced distortion of the STO is visible in the thickness dependence of the full width at half maximum (FWHM) of the XRD rocking curves of the STO

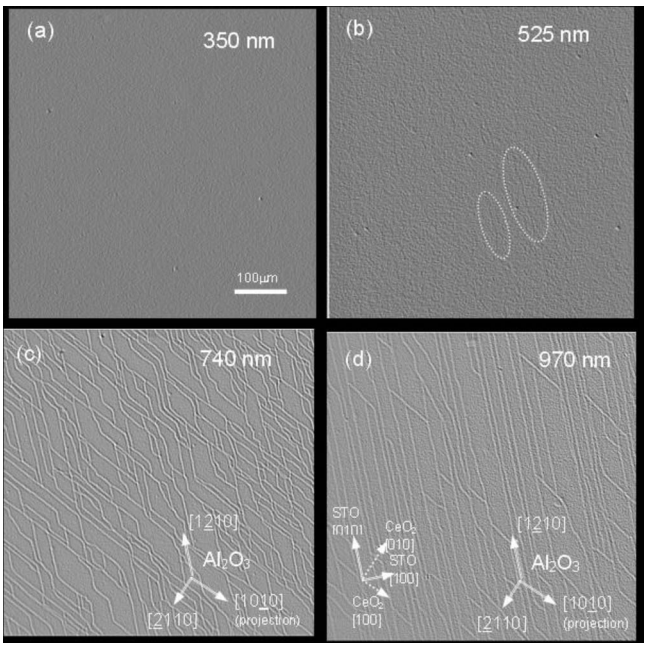

FIG. 3. Microscope images (area: 590×587 μm^2) of the surface of STO films of thickness $d_{STO}=350$ nm (a), 525 nm (b), 740 nm (c), and 970 nm (d). The crystallographic orientations of the substrate, CeO_2 buffer, and STO layer are determined via XRD diffraction experiments, they are identical for all images and are indicated in [(c) and (d)].The dashed ellipses in (b) mark hardly visible cracks in the STO film of medium thickness.

layer (Fig. 2). The XRD data represent the integral properties of the layers. The strain seems to relax over the thickness of the STO layers since thicker films show smaller FWHM values. The relaxation is typically caused by defects, however, for thicker STO layer formation of cracks sets in and leads to additional relaxation of stress. Both mechanisms are discussed below.

Figure 3 displays the surface morphology of four typical samples with STO layer of different thickness. The sample with the thinnest STO layer [$d_{STO}=350$ nm, Fig. 3(a)] shows a smooth surface that is free of cracks. All samples with thinner STO layer ($d_{STO}\leq350$ nm) show similar properties, i.e., smooth surface and no cracks.

In contrast, all thicker STO films ($d_{STO}\geq525$ nm) reveal cracks. For 525 nm [Fig. 3(b)] few cracks with finite lateral extension (typically $\ll200$ μm) are present. All cracks point in the same crystallographic direction, i.e., the [010] direction of STO which is identical to the [$1\bar{2}10$] direction of r-cut sapphire [see also Fig. 4(a)].

The even thicker films ($d_{STO}\geq740$ nm) show a network of cracks. The cracks are oriented along two crystallographic directions, i.e., along the [$1\bar{2}10$] and, additionally, along the [$10\bar{1}0$] direction of the r-cut sapphire. Since there is no distinguished crystallographic orientation of the STO and CeO_2 layers equivalent to the [$10\bar{1}0$] direction of the r-cut sapphire, this indicates that (a) the cracks are generated by the difference of the expansion coefficient of sapphire and STO, and (b) that the (in-plane) expansion coefficient of sapphire is slightly anisotropic. This will be discussed in detail below.

Figure 4 shows characteristic XRD data obtained for the STO films of different thickness. A characteristic set of pole figures [Fig. 4(a)] reveals the in-plane crystallographic orien-

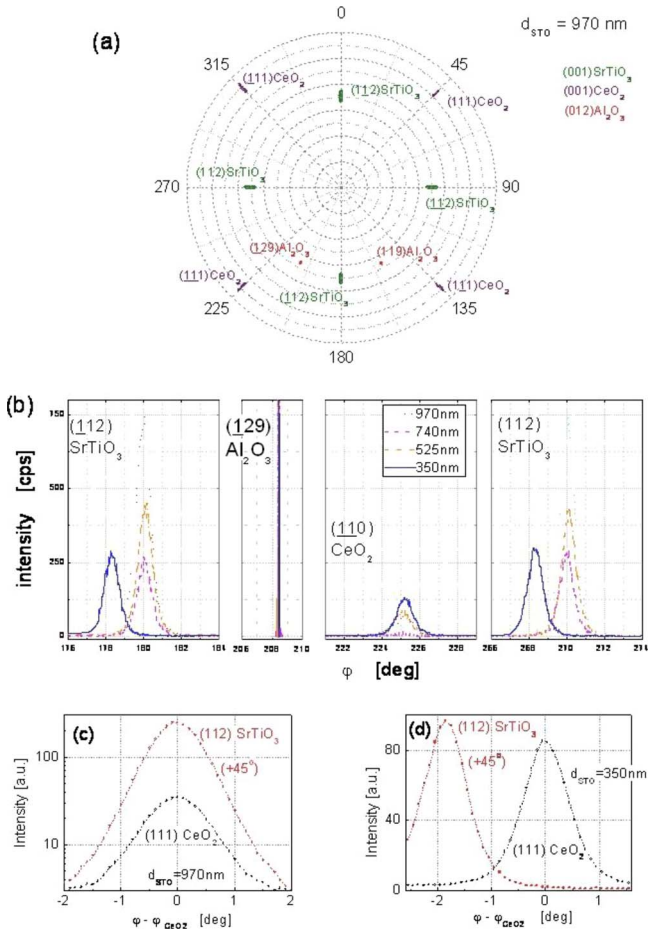

FIG. 4. (Color online) (a) XRD pole figures [(001) STO, (001) CeO_2, and (012) Al_2O_3] provide the in-plane crystallographic orientation of the different layers with respect to the orientation of the substrate; (b) 2D-plot of the φ dependence of characteristic diffraction peaks of the pole figures [(112) and ($1\underline{1}2$) of STO, ($1\underline{1}0$) of CeO_2, and ($1\underline{2}9$) of Al_2O_3] obtained for the samples of different STO layer thicknesses. The characteristic shift in the STO diffraction peak with respect to the CeO_2 diffraction peak is shown in detail for a thick film (c) and a thin film (d). For a better comparison, the (112) STO peaks are shifted by 45° in [(c) and (d)].

tation of the different layers (STO and CeO_2) and the substrate. The φ positions of the different XRD diffraction peaks provide the crystal orientation of the different compounds. Based on these measurements, the crystallographic orientations are indicated in the microscope images in Fig. 3.

All samples show identical mutual crystallographic orientation of the STO, CeO_2 and sapphire. Only thin films ($d \leq 350$ nm) revealed a small shift in the φ position in the STO peak. This is shown in Figs. 4(b)–4(d). Figure 4(b) shows a comparison of the φ positions of two STO peaks [(112) and ($1\underline{1}2$)], ($1\underline{1}0$) of CeO_2 and ($1\underline{2}9$) of Al_2O_3, respectively. The positions of the different peaks are identical (within the experimental accuracy). Only the STO peaks for the thinnest sample are shifted toward smaller angles. This situation is shown in detail in Figs. 4(c) and 4(d). Figure 4(c) shows the crystalline orientation between CeO_2 and STO for thick STO films. The diffraction peaks of (111) CeO_2 and (112) STO differ by exactly 45° which demonstrates the expected in-plane orientation of epitaxial STO on CeO_2. In the case of thin STO films, the STO peaks are additionally shifted (for the 350 nm thick STO film by $\sim -1.9°$) with respect to the standard 45° rotation of STO and CeO_2 in-plane orientation [Fig. 4(d)]. This additional shift in the φ positions is present in all thin films. It indicates that the crystallographic structure of the thin STO films is distorted in the plane, whereas the out-of-plane lattice parameter is not affected (Fig. 2). These observations confirm the presence of in-plane strain in thin STO layers on CeO_2 buffered sapphire. Furthermore, it nicely agrees with the observation of cracks developing for thick films (Fig. 3) and the induced ferroelectricity (Fig. 1) that is reported in literature.[9] In the following we will discuss the origin of stress, its impact upon strain and strain relaxation via generation of defects in this system in more detail.

Heteroepitaxial strained-layer growth represents a major technology for advanced semiconductor and correlated devices and for structures for solid state research. Nevertheless, the most fundamental questions in strained-layer growth are (i) up to what thickness are heteroepitaxial layers stable, (ii) which type of misfit defects develop, and (iii) what happens upon modifications of the misfit for instance due to cooling of the film?

Generally it is believed that below a critical thickness the strained state is the thermodynamic equilibrium state, and above a critical thickness a strained layer may be metastable or it may relax.[13] Different critical thicknesses might be associated to different types of misfit defects, e.g., dislocations, misalignments, or even cracks.[14] Stress σ in heteroepitaxially grown films generally results from the lattice mismatch between the substrate and the thin film. Due to the growth process, this effect can be divided two components: an intrinsic component and a temperature-dependent component. The main reason for the development of intrinsic stress in heteroepitaxially grown films is given by the nominal lattice mismatch $\varepsilon_o = (a_{\text{film}} - a_{\text{substrate}})/a_{\text{film}}$ at growth condition,[13,14] where a represents the lattice parameter of the film and substrate at given condition (e.g., elevated growth temperature), respectively. The thermal contribution to the stress arises from the difference in thermal expansion coefficient of the film and the underlying substrate. Thus, the resulting modified strain is given by[15–17]

$$\varepsilon_o(T) = \frac{a_{\text{film}}(T) - a_{\text{substrate}}(T)}{a_{\text{film}}(T)}. \tag{1}$$

Due to the two contributions, the generation of defects in our heteroepitaxial STO films can be discussed in two steps:

(i) generation of lattice misfit dislocations during the growth of STO at elevated temperature (850 °C); and
(ii) generation of cracks that are most likely generated during the cooling down after deposition.

Ad (i): During the growth, defect-free films grow up to a critical thickness d_c. Above d_c defects develop in the layer. This situation is most generally described initially by van der Merwe[18] and later by Matthews and Blakeslee.[19] In these theories, the line tension of a misfit dislocation of finite length is balanced by the force due to the strain in the layer on the termination of the misfit dislocation. Alternatively and equivalently, the energy of the system with and without the

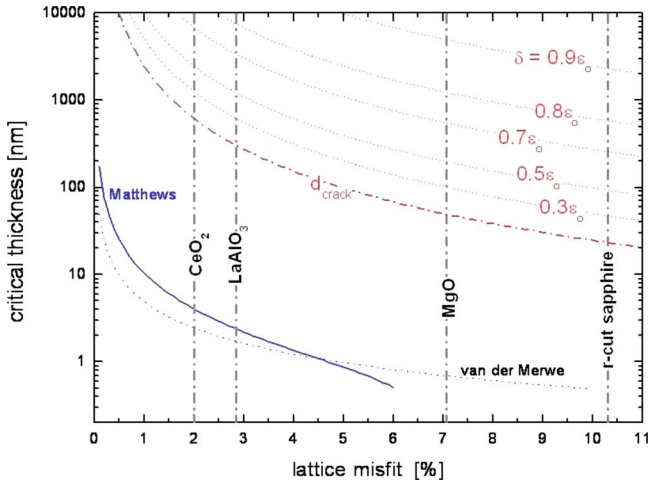

FIG. 5. (Color online) Critical thicknesses for the generation of misfit dislocations according to van der Merwe (Ref. 18) (dotted black line) and Matthews theory [solid line, Eq. (3)], and critical thickness for crack generation according to Eq. (6) for different values of δ and $E'_{\text{surface}}=23\ \text{J/m}^2$. The vertical lines indicate the lattice misfit of STO with respect to various substrates.

misfit dislocation may be considered.[20–22] Although in either approaches several approximations of uncertain effect are made, reasonable values for the critical thicknesses are obtained that are comparable to experimental values[23] and provided the basis for the discussion of defect development in various heteroepitaxial grown film systems, e.g., semiconductor films. For instance the Matthews theory predicts a critical thickness for the development of dislocation lines according to[19]

$$d_c = \frac{C}{\varepsilon_o(T_{\text{growth}})}\ln\{O(d_c)\}, \tag{2}$$

where C contains the details of the crystal and the dislocation, and T_{growth} represents the growth temperature. Different versions of the term $O\{d_c\}$ within the logarithm are discussed by different authors,[13,20,21,23] the resulting predictions of critical thickness can vary by at least a factor of 2. For instance the development of misfit dislocation lines has been described with this approach by[23]

$$d_c \cong \left[\frac{b}{4\pi(1+\nu)\varepsilon_o}\right]\left[\ln\left(\frac{d_c}{b}\right)+1\right], \tag{3}$$

where b and ν represent the extension of the dislocation line and Poisson's ratio, respectively.

Typical predictions for the critical thickness describing the development of misfit dislocations in STO are given in Fig. 5. Inserting reasonable values into Eq. (3) we can estimate the critical thickness for our film system. For STO on CeO_2 (2% misfit) we expect $d_c<10$ nm. The misfit between the buffer layer and r-cut sapphire is even larger ($\varepsilon_o \approx 8.5\%$), $d_c<1$ nm is expected for CeO_2 on sapphire. Therefore a large numbers of misfit dislocations will be created in the CeO_2 buffer layer and the STO layer during growth. These defects reduce the misfit stress in the STO/CeO_2 film system.

This situation can be observed in our films. The width of the XRD rocking curves is indicative for the amount of dislocations in the layer. Extremely large FWHM values are observed for the thin CeO_2 buffer layers ($\Delta\rho_{(001)CeO_2}=0.98°$) and for the thin STO films ($\Delta\rho_{(200)STO}\approx 1-1.2°$, see Fig. 2). With increasing layer thickness, the strain relaxed due to the misfit dislocations and the crystalline quality improves. As a result the width of the rocking curve (representing an integral value of the crystalline quality of the layer) decreases. This is observed for the STO layers. The FWHM value decreases with thickness from $\sim 1°$ for $d<20$ nm to $\sim 0.4°$ for $d>400$ nm (Fig. 2). Furthermore, the generation of defects in CeO_2 on sapphire has been shown in TEM experiments. Large numbers of misfit dislocations are visible in CeO_2 layer starting only a few atomic layers above the CeO_2—sapphire interface.

Ad (ii): After deposition of the STO layer at elevated temperature (850 °C) the sample is cooled down to room temperature. Due to the mismatch of the thermal expansion coefficient, additional stress is imposed on the STO layer. Taking into account the presence of misfit dislocations generated during the growth process, the resulting strain imposed on the film can be described by[14,21]

$$\varepsilon_{\text{film}}(T) = \varepsilon_o(T) - \delta = \left|\frac{a_{\text{film}}(T) - a_{\text{substrate}}(T)}{a_{\text{film}}(T)}\right| - \delta, \tag{4}$$

where δ describes the release of stain due to the presence of defects or misalignments. While defects and misalignments have developed during growth, cracks are expected to develop during cool down if these are energetically favorable. According to the theory of fracture of solids, the amount of strain energy that is released per unit length of a two-dimensional crack is given by[14,24]

$$E_{\text{crack}} = \pi Y \varepsilon^2 \left(\frac{d}{2}\right)^2, \tag{5}$$

where d represents the height of the crack (defined by the thickness of the film, if the crack is normal to the film surface) and Y is the Young modulus of the material. The Young's modulus of bulk $SrTiO_3$ amounts to $Y=238$ GPa if single crystal data are averaged.[25] The formation of a crack is energetically favorable, if E_{crack} exceeds the energy $2E_{\text{surface}}$ (energy per unit crack length) required for the (initial) formation of the two new surfaces of the crack. Therefore, the critical film thickness for crack formation is given for $E_{\text{crack}}=2E_{\text{surface}}$

$$d_{\text{crack}} = \frac{8E'_{\text{surface}}}{\pi Y \varepsilon^2}, \tag{6}$$

with $E'_{\text{surface}}=E_{\text{surface}}/d$. On the one hand, the energy of the crack's surface can be estimated by summation of the binding energies E_B of all atoms at the surface. Generally binding energies of oxides are of the order of 15 eV,[14] values of $E_B=10-12$ eV are reported for STO crystals.[26] The resulting surface energy for cracks along [100], [010], or [001] axes of STO results in a surface formation energy $E'_{\text{surface}} \approx 23\ \text{J/m}^2$. This value represents the ideal situation, i.e., the maximum possible surface formation energy. In this theoretical approach neither the impact of defects are considered nor is the situation of a gradual developing of the rupture and

reorganization of the developing surfaces included. The value describes the uniform formation of the complete and defect free surface. On the other hand, experimental values for the formation of a surface describe the situation including defects and the gradual disjunction of the material including reorganization of the surface. Typical experimental values for surface formation in metallic films range between 1 and 4 J/m^2.[27,28] Experimental values for oxides are not reported according to our knowledge. Considering the problems of the different approaches, theoretical and experimental values are quite similar. The real value for the formation of crack should lie between both values.

Figure 5 shows the resulting critical thickness d_{crack} for different values of δ (in units of ε_o) and a surface formation energy of $E'_{surface}=23\ J/m^2$. The derived values of d_{crack} are comparable with experimental observation for epitaxial oxide layers in general. Ideal, defect-free films show the smallest critical thickness. For a misfit of 10% (e.g., STO on sapphire) crack-free layers are limited by $d_{crack}<30$ nm. With increasing δ the critical thickness increases.

Our films obviously possess defects that are generated during the growth (see discussion above). As a result, $\delta>0$ and the critical thickness are enhanced with respect to the critical thicknesses of defect-free STO films. Therefore:

(i) Films that are thinner than the critical thickness, $d_{STO}<d_{crack}(\delta)\approx 500$ nm in our case, show no cracks upon cooling after deposition. The stress (intrinsic and thermal) is compensated by misfit dislocations generated during growth and a deformation of the STO lattice [see Fig. 4(d)].

(ii) For films with $d>d_{crack}$, cracks develop. This situation is observed in our case for $d_{STO}>500$ nm. However, there seems to be a predominant orientation of the first type of cracks. They develop in $[1\underline{2}10]$ direction of the r-cut sapphire. Either thermal induced lattice mismatch is largest perpendicular to this direction, or the fact that this crystalline direction in sapphire coincides with the [010] crystalline direction in STO, leads to this orientation of the first cracks. As a consequence of the cracks, the remaining stress of the STO is relaxed, no deformation of the STO lattice is observed in XRD pole figures [see Figs. 4(b) and 4(c)].

(iii) For the largest STO films (in our case: $d_{STO}>700$ nm), crack formation takes place in two directions, i.e., along the $[1\underline{2}10]$ and, additionally, the $[10\underline{1}0]$ direction of the r-cut sapphire. Now the thermally induced mismatch seems to be sufficient to induce cracks also in the second direction that is not identical to a crystalline direction STO. As in the previous case (ii), the STO relaxes and no deformation of the STO lattice is observed [see Figs. 4(b) and 4(c)].

III. CONCLUSIONS

We demonstrated that intrinsic and thermal induced stress are important for the understanding of structural modifications and formation of defects in heteroepitaxially grown STO films on sapphire. A model was developed to describe (i) the generation of misfit dislocations during growth and (ii) the crack formation during cooling of the sample. These processes are generated by misfit of the lattice constant and misfit of the thermal expansion coefficient that define two critical thicknesses for the generation of dislocations and cracks, respectively. The results demonstrate that intrinsic mismatch and thermal mismatch have to be considered to explain strain dependent effects in complex heteroepitaxial layer systems like induced ferroelectricity in STO on sapphire.[9] The model on its own and the experimental data reported for STO on sapphire demonstrate that misfit in lattice constant and thermal expansion can be a powerful tool to engineer the properties of heteroepitaxial films, especially, the ferroelectric properties of STO.

ACKNOWLEDGMENTS

The authors would like to thank H.P. Bochem, M. Nonn, A. Zaitsev, N. Klein, and A. Offenhäuser for their valuable support.

[1] G. A. Gehring and K. A. Gehring, Rep. Prog. Phys. **38**, 1 (1975); R. S. Beach, J. A. Borchers, A. Matheny, R. W. Erwin, M. B. Salamon, B. Everitt, K. Pettit, J. J. Rhyne, and C. P. Flynn, Phys. Rev. Lett. **70**, 3502 (1993); Q. Gan, R. A. Rao, C. B. Eom, J. L. Garrett, and M. Lee, Appl. Phys. Lett. **72**, 978 (1998).
[2] J. M. Lock, Proc. R. Soc. London, Ser. A **208**, 391 (1951); H. Sato and M. Naito, Physica C **274**, 221 (1997); I. Bozovic, G. Logvenov, I. Belca, B. Narimbetov, and I. Sveklo, Phys. Rev. Lett. **89**, 107001 (2002).
[3] A. F. Devonshire, Philos. Mag., Suppl. **3**, 85 (1954).
[4] G. A. Samara, Ferroelectrics **2**, 277 (1971).
[5] G. A. Rossetti, Jr., L. E. Cross, and K. Kushida, Appl. Phys. Lett. **59**, 2524 (1991).
[6] K. Abe, N. Yanase, K. Sano, M. Izuha, N. Fukushima, and T. Kawakubo, Integr. Ferroelectr. **21**, 197 (1998).
[7] S. K. Streiffer, J. A. Eastman, D. D. Fong, C. Thompson, A. Munkholm, M. V. Ramana Murty, O. Auciello, G. R. Bai, and G. B. Stephenson, Phys. Rev. Lett. **89**, 067601 (2002).
[8] J. H. Haeni, P. Irvin, W. Chang, R. Uecker, P. Reiche, Y. L. Li, S. Choudhury, W. Tian, M. E. Hawley, B. Craigo, A. K. Tagantsev, X. Q. Pan, S. K. Streiffer, L. Q. Chen, S. W. Kirchoefer, J. Levy, and D. G. Schlom, Nature (London) **430**, 758 (2004).
[9] R. Wördenweber, E. Hollmann, R. Kutzner, and J. Schubert, J. Appl. Phys. **102**, 044119 (2007).
[10] R. Wördenweber, E. Hollmann, M. Ali, J. Schubert, G. Pickartz, and T. K. Lee, J. Eur. Ceram. Soc. **27**, 2899 (2007).
[11] N. A. Pertsev, A. K. Tagantsev, and N. Setter, Phys. Rev. B **61**, R825 (2000); **65**, 219901(E) (2002).
[12] International Centre for Diffraction Data, Powder Diffraction File Database, Sets 1–45, Data Nos. 07–204, 21–972, 34–394.
[13] J. R. Downes, D. J. Dunstan, and D. A. Faux, Semicond. Sci. Technol. **9**, 1265 (1994).
[14] A. G. Zaitsev, G. Ockenfuß, and R. Wördenweber, Inst. Phys. Conf. Ser. **158**, 25 (1997).
[15] M. Ohring, *The Materials Science of Thin Films* (Academic, New York, 1991).
[16] R. W. Hoffman, Thin Solid Films **34**, 185 (1976).
[17] T. R. Taylor, P. J. Hansen, B. Acikel, N. Pervez, R. A. York, S. K. Streiffer, and J. S. Speck, Appl. Phys. Lett. **80**, 1978 (2002).
[18] J. H. Van der Merwe, J. Appl. Phys. **34**, 123 (1963).
[19] J. W. Matthews and A. E. Blakeslee, J. Cryst. Growth **27**, 118 (1974).
[20] S. M. Hu, J. Appl. Phys. **69**, 7901 (1991).

[21]E. A. Fitzgerald, Mater. Sci. Rep. **7**, 87 (1991).
[22]L. B. Freund, J. Mech. Phys. Solids **38**, 657 (1990).
[23]R. People and J. C. Bean, Appl. Phys. Lett. **47**, 322 (1985).
[24]A. H. Cottrell, in *Physics of Metals: Defects*, edited by P. B. Hirsch (Cambridge University Press, Cambridge, 1975), Vol. 2.
[25]P. Paufler, B. Bergk, M. Reibold, A. Belger, N. Pätzke, and D.C. Meyer, Solid State Sci. **8**, 782 (2006) and Ref. 20 therein.
[26]C. Webb and M. Lichtensteiger, Surf. Sci. **107**, L345 (1981).
[27]P. F. Becher and J. S. Murrday, J. Mater. Sci. **12**, 1088 (1977).
[28]H. Ji, G. S. Was, and M. D. Thouless, Eng. Fract. Mech. **61**, 163 (1998).